Structures and Buildings
(Proceedings of the ICE)

Dynamic response and progressive collapse resistance of RC flat slab structures following instantaneous column removal

STBU-2025-199 | Paper

Submitted on: 27-09-25

Submitted by: Bo Wei,Pengfei Xiao,Feng Fu,Zhi Li

Keywords: DYNAMICS,BUILDINGS, STRUCTURES & DESIGN,FLAT SLAB STRUCTURE,REINFORCED CONCRETE,PUNCHING SHEAR,PROGRESSIVE COLLAPSE,DYNAMIC RESPONSE


RIVER VALLEY
TECHNOLOGIES

Written: 28 August 2025

Manuscript title: Dynamic response and progressive collapse resistance of RC flat slab structures following instantaneous column removal

Authors: Bo Wei[1,3], Pengfei Xiao[2], Feng Fu[1,4], Zhi Li[1,2]

Affiliations: [1]Guangxi Key Laboratory of Green Building Materials and Construction Industrialization, Guilin University of Technology, Guilin, China and [2]College of Civil Engineering, Guilin University of Technology, Guilin, China and [3]Nanning Industrial Park Investment and Development Group Co., Ltd, Nanning, China and [4]Department of Engineering, School of Science and Technology, City, University of London, UK, EC1V,0HB

Corresponding author: Zhi Li, Guangxi Key Laboratory of Green Building Materials and Construction Industrialization, Guilin University of Technology, Guilin, China

E-mail: Lizhi@glut.edu.cn

Abstract

Quasi-static investigations have demonstrated that continuous reinforcement traversing the columns enhances the load-bearing capacity of reinforced concrete (RC) flat slab systems subjected to progressive collapse initiated by column removal. Nevertheless, the dynamic behavior of older structures lacking reinforcement remains insufficiently understood. To address this gap, high-fidelity numerical models were developed in LS-DYNA and validated against experimental data. Additionally, this study examined the load redistribution and internal force transfer mechanisms. The results revealed that following the removal of a central column, inertial effects amplified the applied load by a factor of 1.12, with more than 60% of the load ultimately redistributed to the edge columns. In addition, the influence of varying column removal scenarios and structural scales on the dynamic response and collapse resistance of flat slab systems was explored. Findings indicate that the simultaneous loss of opposite edge columns imposes a greater collapse risk than the concurrent loss of adjacent edge columns. Moreover, the evaluation results of scaled RC flat slab structures tend to overestimate both their dynamic load-bearing capacity and punching shear resistance.

Keywords: Flat slab structure; Reinforced concrete; Punching shear; Progressive collapse; Dynamic response

1. Introduction

Progressive collapse refers to a disproportionate structural failure triggered by localized damage induced by accidental loads (ASCE 2010). It develops when the remaining structure is unable to form effective alternative load paths, thereby allowing damage to propagate throughout the system. Historical catastrophic failures, such as the 1971 collapse of the 2000 Commonwealth Avenue building in the United States (King and Delatte 2004), the 1995 failure of the Sampoong Department Store in South Korea (Gardner *et al*. 2002), and the 2001 World Trade Center collapse (Bažant and Verdure 2007), underscore the severe consequences of disregarding progressive collapse in structural design.

Extensive research has examined the progressive collapse resistance of reinforced concrete (RC) frame structures (Ju and Kwak 2023; Miceli and Castaldo 2024; Miceli *et al*. 2025; Qian *et al*. 2021; Wang *et al*. 2022; Yi *et al*. 2021; Yi *et al*. 2024; Zhang and Li 2020). In contrast, flat slab systems lack beams, which severely limits their ability to redistribute loads. This intrinsic weakness renders slab–column connections particularly susceptible to punching shear failure, thereby markedly elevating the risk of progressive collapse (Qian and Li 2013). Consequently, a systematic investigation into the progressive collapse resistance of RC flat slab systems is essential (Xue *et al*. 2018).

Qian and Li (2013) were the first to experimentally evaluate the influence of drop panels on the progressive collapse resistance of flat slab systems, reporting that the first peak load increased by 124.7% with the inclusion of drop panels. Subsequently, Qian

and Li (2015a) revealed the load resisting mechanism to mitigate progressive collapse of flat slab structures. Yi *et al*. (2014) performed quasi-static tests to assess the progressive collapse resistance of flat slab systems under various column removal scenarios. Their findings demonstrated that compression and tension membrane actions constitute the primary resistance mechanisms following column removal, and that failure is more likely when corner or edge columns are lost compared with interior columns. Similarly, Ma *et al*. (2019, 2020) examined progressive collapse under different removal scenarios and concluded that the concurrent loss of interior and edge columns poses a greater risk than the removal of edge columns alone. Qian and Li (2016) first investigated the failure modes and load-resisting mechanisms of flat slab structures in different phases. Furthermore, Qian *et al*. (2018) firstly revealed the load resisting mechanism to mitigate progressive collapse of flat slab structures under multiple column failures. Weng *et al*. (2020) conducted numerical analyses on the role of continuous reinforcement in columns, innovatively revealing that the post-punching capacity of flat slab systems is predominantly governed by the extent of reinforcement continuity. These studies employed the quasi-static pushdown method, which is effective in elucidating resistance mechanisms and load redistribution following column loss. However, actual column removal typically occurs instantaneously (Russell *et al*. 2015), introducing dynamic amplification of bending moments and shear forces. This effect substantially elevates the risk of punching shear failure in the surrounding connections, potentially triggering the progressive collapse of the slab system. Qian and Li (2015b) conducted pioneering experimental and numerical studies

on dynamic responses under instantaneous column removal, demonstrating that drop panels effectively reduce punching shear risks. Peng *et al*. (2017, 2018) performed dynamic tests on slab systems without continuous column reinforcement and observed increased susceptibility to progressive collapse. Similarly, Adam *et al*. (2020) conducted full-scale dynamic tests under corner column removal scenarios and observed that the flexural mechanism was the primary resistance prior to punching shear failure. In addition, various methods have been proposed to enhance the progressive collapse resistance of flat slab structures. Qian and Li (2015c) were first to adopt GFRP strips as a strengthening technique, showing that the proposed method significantly improves collapse resistance. In recent years, research has expanded to consider multi-hazard conditions. For instance, Qian *et al*. (2022a, 2022b) and Weng *et al*. (2023) systematically investigated the effects of rebar corrosion on the punching shear strength of slab-column connections. Furthermore, Qian *et al*. (2024) and Lan *et al*. (2025) proposed the use of hybrid BFRP and steel bar to mitigate the impact of corrosion on the punching shear capacity of slab-column connections, demonstrating its effectiveness in enhancing durability. More recently, Weng *et al*. (2025) conducted pioneering research on the post-fire punching shear behavior of full-scale reinforced concrete slab-column connections.

In conclusion, although quasi-static analyses in previous studies have shown that continuous reinforcement through columns markedly improves the progressive collapse resistance of flat slab systems, the dynamic behavior under sudden column loss—particularly in older structures lacking such reinforcement—remains insufficiently

explored. Prior to the 2005 revision of ACI 318 [American Concrete Institute (ACI) 1971, 2005], the absence of code-mandated continuous reinforcement rendered flat slab systems highly vulnerable to progressive collapse. Accordingly, detailed investigations of these systems under sudden column removal scenarios are critically important. Building on the dynamic tests conducted by Peng et al. (2017, 2018), this study developed a high-fidelity numerical model for RC flat slab systems without continuous reinforcement. After validating the accuracy of the model, the study examined load redistribution and evolution of internal forces in critical slab regions. In addition, a parametric analysis was performed to quantify the influence of column removal scenarios (single-and multi-column loss) and structural scaling on the structural response.

2. FE modeling

2.1. Brief of test program

This section presents numerical simulations replicating the test of Peng *et al*. (2017, 2018) to validate the accuracy and reliability of the model adopted in this study.

Peng *et al*. (2017, 2018) conducted dynamic tests on 2/5-scale, single-story flat slab systems with a 2×2 bay configuration, considering two column removal scenarios: edge column (B1) and middle column (B2) removal. The specimen geometry and reinforcement details are shown in **Figure 1**. The rebars exhibited yield strength and ultimate strength of 655 MPa and 737 MPa, respectively, with an elongation of approximately 4.0%. The measured concrete compressive strengths were 32.7 MPa and 30 MPa for the edge and middle column removal scenarios, respectively. For more

details on specimen design and material properties, refer to Peng *et al*. (2017, 2018).

The experimental setup is shown in **Figure 2**. For the edge column removal scenario, uniform loads of 4.83 kN/m² were applied to the interior area and 11.40 kN/m² to the extended area (Peng *et al*., 2017). For the interior column removal scenario, the corresponding applied loads were 5.55 kN/m² and 15.51 kN/m², respectively (Peng *et al*., 2018).

2.2 Element type and boundary conditions

The commercial software LS-DYNA was used for the numerical analysis, given its numerical stability and extensive library of constitutive models (Wu *et al*., 2012). The entire 2×2 bay structure was modeled. However, owing to symmetry, only one-quarter of the model was presented. As shown in **Figure 3**, the numerical models were constructed to replicate the experimental specimens. It is noted that the models for the edge and interior column removal cases were identical, differing only in the applied loads.

Concrete was modeled using 8-node solid elements (SOLID164) with reduced integration. With appropriate hourglass control, this element type provides adequate accuracy while reducing the computational cost. To ensure that hourglass energy remained below 10% of the total internal energy, the Flanagan–Belytschko stiffness formulation with exact volume integration was adopted, with the hourglass coefficient set to 0.002. The steel columns were also modeled using explicit solid elements. The reinforcement was represented by 2-node Hughes–Liu beam elements (BEAM161) with 2×2 Gauss quadrature integration, which effectively captured the mechanical

behavior of the rebars, including axial force, biaxial bending, and transverse shear.

The longitudinal rebars of RC columns were tied to the steel column by using the keyword *CONTACT_TIED_NODES_TO_SURFACE. Moreover, previous studies have indicated that assuming perfect bonding between rebars and concrete ensures sufficient reliability for the numerical simulation of RC structures against progressive collapse (Weng *et al*., 2020). Thus, *CONSTRAINED_LAGRANGE_IN_SOLID was chosen for defining the relationship between concrete and rebars. Furthermore, the keyword *AUTOMATIC_GENERAL was employed to prevent numerical penetration between adjacent reinforcement elements during the large deformation stages, ensuring solution stability.

2.3 Material model

The Continuous Surface Cap Model (CSCM) was employed to simulate the concrete behavior (Wu *et al*., 2012). The CSCM can effectively capture the response of concrete under low confinement, including damage-induced softening, modulus reduction, shear dilation, compaction, confinement, and strain rate effects. The original CSCM (*MAT_CSCM) requires numerous input parameters. However, LS-DYNA also provides a simplified version (*MAT_CSCM_CONCRETE), applicable for concrete with unconfined compressive strength between 28 MPa and 48 MPa. This simplified model requires only three inputs: unconfined compressive strength f_c, maximum aggregate size A_g, and units, whereas the remaining parameters are automatically generated according to the CEB-FIP (1991) model code. The measured compressive strengths of the two test specimens were 32.7 MPa and 30 MPa, respectively. An

167 average value of 31.4 MPa was adopted in the simulations, with a maximum aggregate
168 size of 10 mm. The strain rate effect was considered by setting IRATE = 1. To simulate
169 material failure, the CSCM incorporates an erosion algorithm based on the maximum
170 principal strain, and elements are deleted once their principal strain exceeds the defined
171 threshold. However, relying solely on this criterion is insufficient for reproducing
172 punching shear failure. Therefore, in this study, both the maximum effective strain and
173 shear strain criteria were incorporated via *MAT_ADD_EROSION. Specifically, a
174 maximum shear strain ($\gamma_{c,max}$) was applied to a critical punching area of 425 mm×425
175 mm, whereas the maximum effective strain ($\varepsilon_{c,max}$) was assigned to the remaining slab
176 regions to capture flexural failure. As shown in **Figure 3**, the punching area was
177 determined according to ACI 318R-19 (ACI 2019), defined as the column width plus
178 four times the effective slab depth (152 mm+4×66.5 mm = 418 mm). Considering the
179 25 mm mesh size, the region was extended to 425 mm. Finally, the failure thresholds
180 for maximum effective strain and shear strain were calibrated to 0.06 and 0.08,
181 respectively, through iterative simulations of the interior column removal scenario.
182 The reinforcement was modeled using a bilinear elastic–plastic constitutive law
183 (*MAT_PLASTIC_KINEMATIC), as shown in **Figure 4**. The material parameters,
184 including elastic modulus, yield strength, tangential modulus, and ultimate strain, were
185 determined based on experimental test results, while the remaining parameters are
186 summarized in **Table 1**. In this model, the hardening parameter BETA was set to 1,
187 which corresponds to isotropic hardening. The strain rate parameters SRC and SRP
188 were set to 3.2 ms^{-1} and 5, respectively, according to the recommendations of Liu et al.

(2018). The beam element size was set to 30 mm.

2.4 Loading method

The gravity loads acting on the slab were simulated using the keywords *ELEMENT_MASS and *LOAD_BODY_Y, with the total mass uniformly distributed among the slab elements. The quick-release device was simplified by modeling only the bottom steel column, thereby replicating the release stage of either edge or interior columns.

3. FE model verification

3.1 Comparison of crack pattern

Figure 5 presents the comparison of test and numerical crack patterns for the edge column (B1) removal scenario. In both cases, cracks are observed at the top surface of the slab, predominantly concentrated around the removed column. In contrast, only a limited number of cracks appeared at the C3 and A3 column connections, which were farther from the removed column. These observations demonstrate that the numerical model provides an accurate prediction of the crack distribution in flat slab structures subjected to edge column removal.

As shown in **Figure 6**, the model accurately reproduces the crack distribution after the removal of the interior column (B2). After column B2 was removed, punching shear failures developed at the four adjacent columns (A2, B1, B3, and C2), accompanied by closed-ring cracks encircling their peripheries. These results demonstrate that the numerical model can reliably predict the crack distribution in flat slab structures subjected to interior column removal.

3.2 Comparison of Reaction force-history curve

Figure 7 compares the test and numerical simulation curves of the failed column's reaction force history under different column removal scenarios. A gradual load decay phase was observed in the tests, mainly caused by the activation delay of the pneumatic valve and the response time of the hydraulic jack (Peng *et al*., 2018), which did not occur in the simulations. However, the simulated reaction force-history curves showed close agreement with the experimental results, indicating that the numerical model can accurately simulate the sudden column removal of structures.

3.3 Comparison of vertical displacement-history curve

The experimental and numerical vertical displacement-time responses are compared in **Figure 8** and **Table 2**. The numerical results indicate close agreement with the experimental data for inflection point displacement, steady displacement, and the overall development trend. As summarized in **Table 2**, the simulated inflection point and steady displacements deviate by less than 3% from the test results. These findings demonstrate that the numerical model can reliably capture the displacement response of structures under different sudden column removal scenarios.

4. Redistribution of load and internal force

4.1 Load redistribution

Figure 9 illustrates the evolution of residual axial forces following the loss of column B2. Immediately after failure, the total axial force carried by the surrounding columns dropped below the pre-removal value, as the load initially supported by B2 did not instantaneously redistribute but was partly transformed into inertial forces

induced by the downward displacement of the slab. Subsequently, the combined axial force in the remaining columns peaked at 262.1 kN, approximately 1.12 times the total design load. This amplification is attributed to the reaction forces mobilized in adjacent columns to counteract the inertial effects near the failed column.

Figure 10 shows the evolution of axial force distribution between edge columns (A2, B1, B3, and C2) and corner columns (A1, A3, C1, and C3) during structural deformation. As indicated in **Figure 7**, column B2 initially carried 41.3 kN, which was dynamically redistributed upon its removal. Prior to punching shear failure, inertial effects drove the combined axial force in edge and corner columns to 96.6% of the pre-removal level. Among these, the edge columns experienced a 15.6% increase in axial force, whereas the corner columns exhibited a slight reduction. This divergence arises from the rhombus-shaped deformation pattern between edge columns (**Figure 11**), where the slab's downward displacement near column B2 induces upward rotational tendencies at the corners, thereby alleviating part of their axial demand.

After punching shear failure of the edge columns, secondary load redistribution elevated the corner column forces to 108.2% of their initial values. Ultimately, under the stabilized loading condition, more than 60% of the demand originally carried by column B2 was transferred to the edge columns.

4.2 Internal force of slab strip

To examine the internal force transfer mechanism during interior column failure, reinforcement stress distributions at critical slab strip sections were analyzed using the FE model. The locations of these sections and the corresponding reinforcement stresses

255 are illustrated in **Figure 12**. In **Figure 13**, S1-T denotes the top reinforcement at section
256 S1, and S1-B denotes the bottom reinforcement at section S1.

257 As shown in **Figure 13**, during the initial stage of column B2 removal,
258 reinforcement stresses near the failed column were primarily compressive. With
259 increasing deformation in the B2 region, the compressive stresses in the top slab
260 reinforcement first intensified and then transitioned to tensile stresses. This transition
261 signifies the development of pronounced tensile membrane action within the structure.

262 In section S3, the bottom reinforcement underwent rupture, whereas the
263 reinforcement at other sections remained intact. This localized failure was attributed to
264 the bending moment distribution along the longitudinal slab strip under uniform loading.
265 The analytical results indicated that the maximum bending moment occurred
266 approximately 38 mm away from the center of column B2 toward column B1, as
267 illustrated in **Figure 14**.

268 **5. Parameter analysis**

269 *5.1 Effect of different column removal scenarios*

270 Since the applied slab loads in Peng *et al*. (2017) differed from those in Peng *et al*.
271 (2018), a direct comparison of structural performance across different column removal
272 scenarios was not feasible. To address this limitation, the B1 column failure specimen
273 was reanalyzed using the design parameters reported by Peng *et al*. (2018). Moreover,
274 prior experimental investigations have primarily focused on single-column failure
275 scenarios, whereas extreme-field events may involve the simultaneous loss of multiple
276 columns. To extend the scope, this study examines the dynamic response of RC flat slab

277 structures under two multi-column failure scenarios: (1) simultaneous failure of an edge
278 column and its adjacent interior column (B1+B2), and (2) simultaneous failure of an
279 edge column and the opposite edge column (B1+C2).

280 **Figure 15** presents the vertical displacement history curves at the failed column
281 locations for different removal scenarios. The research results indicate that different
282 column removal scenarios have a significant effect on the dynamic response of RC flat
283 slab structures. For the single-column removal scenario of B1, the stabilized
284 displacement reached 46 mm, which was 70.8% smaller than that for the single-column
285 removal of B2. This difference arose from the higher initial axial load carried by column
286 B2 (41.3 kN) compared with 15.3 kN for edge column B1, leading to a larger
287 displacement response following the removal of column B2. For the (B1+B2) and
288 (B1+C2) failure scenarios, substantially larger displacements developed under the same
289 applied load, exceeding 180 mm at 0.38s and 0.33s, respectively. Thereafter, the
290 displacements continued to increase until global structural failure occurred.

291 Thus, interior column failure is more critical than edge column failure, and the
292 simultaneous removal of columns (B1+B2) or (B1+C2) precipitates structural collapse.
293 Between these two cases, the (B1+C2) scenario was more severe, as the redistributed
294 loads triggered rapid punching shear failure and reinforcement rupture at the B2
295 connection.

296 **Figure 16** presents the crack patterns for the B1 and B2 column removal scenarios,
297 whereas **Figures. 17** and **18** illustrate the failure modes corresponding to the
298 simultaneous removal of columns (B1+B2) and (B1+C2), respectively. To elucidate the

299 internal force transfer mechanisms under different column failure conditions,
300 reinforcement stresses at critical slab sections were analyzed. **Figure 19** shows the
301 reinforcement stress distribution after the removal of column B1. Along the A1 – C1
302 slab strip, the top reinforcement near column C1 (section S4) developed tensile stresses,
303 whereas the bottom reinforcement was compressed. Conversely, near column B1
304 (section S3), the bottom reinforcement carried tensile stresses, and the top
305 reinforcement was compressed. This pattern indicates that the A1 – C1 strip primarily
306 resisted the loads through flexural action. In contrast, along the B1 – B2 direction, the
307 top reinforcement near column B2 (section S1) experienced tension, whereas the
308 bottom reinforcement was in compression. In section S2, adjacent to column B1,
309 reinforcement stresses remained relatively low, suggesting the development of a
310 cantilever mechanism in this direction. Prior to 0.4 s, the tensile stress in the top
311 reinforcement at section S1 exceeded that at section S4, whereas the compressive stress
312 in the bottom reinforcement at section S1 was lower than that at section S4. This
313 behavior demonstrates that section S1 is subjected to greater internal force demands,
314 progressively approaching a state in which both the top and bottom reinforcements are
315 in tension, signifying the onset of tensile membrane action.

316 **Figure 20** presents the reinforcement stress distribution at critical slab sections
317 following the simultaneous removal of columns (B1+C2). In contrast to the single-
318 column removal of B1, where tensile membrane action is not the governing mechanism,
319 the (B1+C2) scenario induces substantial tensile stresses in most slab reinforcements,
320 ultimately leading to widespread reinforcement fracture. This behavior indicates that

321 although the tensile membrane mechanism is mobilized at an early stage, the high
322 vertical demands subsequently trigger reinforcement rupture, resulting in global
323 collapse.

324 **Figure 21** shows the reinforcement stress distribution at the critical slab sections
325 following the simultaneous removal of columns B1 and B2. The evolution of stresses
326 in the top reinforcement exhibited a trend similar to that observed under the single-edge
327 column removal scenario. Compared with the (B1+C2) removal case, a larger
328 proportion of the reinforcement in the (B1+B2) scenario underwent a sequential
329 transition from compression to tension and ultimately to rupture, suggesting that the
330 structural resistance mechanisms were more extensively mobilized. This observation is
331 consistent with **Figure 15**, where the collapse of the structure following (B1+B2)
332 removal occurs at a slower rate than that associated with (B1+C2) removal.

333 Additionally, **Figure 21** shows that the top reinforcement at sections S1 and S5
334 ruptured almost simultaneously. For the bottom reinforcement, failure initiates at
335 section S1, indicating that the slab region near column B3 sustains the highest internal
336 force demand under the (B1+B2) removal scenario and thus represents the weakest
337 portion of the structure.

338 *5.2 Effect of scale ratio*

339 Given the 2/5-scale test specimens, the size effect on the punching shear behavior
340 of slab – column connections and the influence of specimen mass on the dynamic
341 structural response were investigated through full-scale modeling of the interior column
342 removal case. Additional comparative analyses were performed using the 3/5-scale and

4/5-scale models. For all scaled specimens, the applied load level followed Peng *et al*. (2018), i.e., 1.0DL+0.5LL (6.33 kPa). **Figure 22** presents the pre-removal damage conditions for specimens of different sizes. The full-scale specimen exhibited more severe initial damage than the scaled counterparts, owing to its larger span and mass, with damage severity decreasing proportionally as the scaling ratio decreased. **Figure 23** compares the crack patterns across specimen sizes, showing that surface cracks became more pronounced with increasing specimen size. **Figure 24** illustrates the displacement – time histories after column removal. The results indicate that displacement at the inflection point increases with specimen size, and this increase exceeds the geometric scaling ratio. This phenomenon primarily resulted from the reduced initial damage in the scaled specimens, which enhanced their stiffness and load capacity. Furthermore, it was observed that the structural displacement increased more gradually with increasing specimen size after the inflection point, with the effect being most pronounced in the full-scale model. This behavior arises because larger slab-to-column rotation angles at higher scaling ratios accelerate reinforcement strain development near the connections, leading to earlier rebar fracture. These findings indicate that scaled specimens may not reliably predict the dynamic displacement response and load-bearing capacity of full-scale structures. In particular, scaled models tend to overestimate dynamic performance, especially as the scaling ratio increases. Nevertheless, the failure locations and modes of the scaled specimens remained consistent with those of the full-scale structures.

Punching shear failure is commonly associated with excessive slab-to-column

365 rotations (Muttoni 2008). Following the approach of Peng *et al*. (2018), who derived
366 slab rotation angles from vertical deflections measured 70 mm and 165 mm from the
367 column surfaces, the present study extracted rotation data from validated numerical
368 models. As shown in **Figure 25**, the numerical model accurately reproduced the
369 experimental rotation behavior, including the ultimate rotation angle. **Figure 26**
370 compares the simulated slab rotation curves for different specimen sizes. In this study,
371 punching shear rotation and ultimate rotation are defined as the rotations at the onset of
372 punching shear failure and at the displacement inflection point, respectively. The results
373 demonstrate that the overall trends of the slab rotation curves are consistent across
374 specimen sizes, with rotation increasing sharply once punching shear failure occurs. To
375 further examine the relationship between slab rotation and specimen size, the punching
376 shear and ultimate rotations were plotted against the scaling ratio (**Figure 27**). The
377 results revealed that punching shear rotation decreased with increasing specimen size.
378 Specifically, the 2/5-scale specimen exhibited a punching shear rotation of 0.043 rad,
379 whereas the full-scale specimen exhibited 0.028 rad. This reduction was attributed to
380 the diminished punching capacity of the larger specimens owing to their increased span
381 and thickness. These findings indicate that scaled specimens may overestimate the
382 punching shear capacity of full-scale structures, making them less reliable for
383 predicting dynamic load-bearing capacity. The Department of Defense (DoD 2013)
384 guidelines for progressive collapse prevention consider punching shear failure a brittle
385 limit state and assume non-ductile behavior in connections without continuous
386 reinforcement beyond the punching stage. However, as shown in **Figs. 26** and **27**, slab

rotation continued to increase substantially after punching shear failure. With increasing specimen size, the displacement at the inflection point also increased, leading to larger ultimate rotations. Across all sizes, the ultimate rotation ranged from 0.123 rad to 0.129 rad. This finding suggests that the DoD (2013) guidelines may underestimate the deformation capacity of slab – column connections, particularly with respect to their post-punching deformation behavior.

6. Conclusions

In this study, numerical simulations were conducted to investigate the dynamic response of RC flat slab structures subjected to sudden column removal. From the numerical study results, the following main findings can be drawn:

1. The developed FE model demonstrated a high level of accuracy in simulating the responses of RC flat slab structures subjected to dynamic column removal scenarios. Moreover, the adopted concrete damage criterion effectively captured the punching shear failure at the slab – column connections.
2. The sudden removal of an interior column causes the load previously carried by the failed column to be partially transformed into inertial forces, resulting in a peak axial force in the surrounding columns that reaches 1.12 times the total design load. Ultimately, more than 60% of the original load of the removed column was redistributed to the edge columns.
3. The failure of interior columns induced substantially larger displacements than to edge column failure. Among the two-column failure scenarios, the simultaneous removal of an edge column and its opposite edge column was the most critical, as

409 the redistributed loads triggered rapid punching shear failure and reinforcement
410 rupture at the slab – column connections, thereby expediting the progressive
411 collapse.

412 Finally, although scaled specimens can reasonably capture the failure modes and
413 load redistribution mechanisms of flat slab structures, they are unreliable for
414 quantifying the actual dynamic load-bearing capacity. Owing to scale effects, such
415 specimens consistently overestimate both dynamic capacity and punching shear
416 resistance. Moreover, the DoD (2013) guidelines tend to underestimate the deformation
417 capacity of slab – column connections lacking continuous reinforcement through the
418 column, particularly in the post-punching stage, thereby overlooking the significant
419 ductility observed in practice.

420 **Acknowledgements**

421 This research is supported by the Guangxi Natural Science Foundation (Nos.
422 AD25069101 and 2025GXNSFAA069803), and the National Natural Science
423 Foundation of China (No. 52308489). Any opinions, findings and conclusions
424 expressed in this paper do not necessarily reflect the view of National Natural Science
425 Foundation of China and Guangxi Natural Science Foundation.
426

References

ASCE. (2017). Minimum design loads and associated criteria for buildings and other structures. ASCE 7-16. Reston VA: ASCE.

Adam JM, Buitrago M, Bertolesi E, Sagaseta J and Moragues JJ (2020) Dynamic performance of a real-scale reinforced concrete building test under a corner-column failure scenario. *Engineering Structures* **210**: 110414.

ACI (American Concrete Institute). (1971). Building code requirements for reinforced concrete. *ACI 318-71*, Farmington Hills, MI.

ACI (American Concrete Institute). (2005). Building code requirements for structural concrete and commentary. *ACI 318-05*, Farmington Hills, MI.

ACI (American Concrete Institute). (2019). Building code requirements for structural concrete and commentary. *ACI 318R-19*, Farmington Hills, MI.

Bažant ZP, Verdure M (2007) Mechanics of progressive collapse: Learning from World Trade Center and building demolitions. *Journal of Engineering Mechanics* **133(3)**: 308–319.

CEB. (1991). *CEB - FIP Model Code 1990*. London: Thomas Telford.

DoD (Department of Defense). (2013) Design of buildings to resist disproportionate collapse. *UFC 4-023-03*, Washington, DC.

Gardner NJ, Huh J, Chung L (2002) Lessons from the Sampoong department store collapse. *Cement and Concrete Composites* **24(6)**: 523–529.

Ju S and Kwak HG (2023) Analytical model for progressive collapse of rc frame structures subjected to blast loadings. *Journal of Building Engineering* **71**: 106474.

King S, Delatte NJ (2004) Collapse of 2000 commonwealth avenue: Punching shear case study.

449 *Journal of Performance of Constructed Facilities* **18(1)**: 54–61.

450 Liu K, Liu B, Villavicencio R, Wang Z and Soares CG (2018) Assessment of material strain rate
451 effects on square steel plates under lateral dynamic impact loads. *Ships and Offshore Structures*
452 **13(2)**: 217-225.

453 Lan DQ, Qian K, Weng YH and Yang YW (2025) Punching Shear Behavior of Slab-Column
454 Structures with Hybrid Reinforcements: Experiment, Simulation, and Theoretical Analysis.
455 *Journal of Structural Engineering* **151(6)**: 04025054.

456 Miceli E, De Iuliis M and Castaldo P (2025) Robustness assessment of reinforced concrete structures
457 for different failure scenarios. *Structural Concrete.*

458 Miceli E and Castaldo P (2024) Robustness improvements for 2D RC moment resisting frames:
459 parametric study by means of NLFE analyses. *Structural Concrete* **25(1)**: 9-31.

460 Ma F, Gilbert BP, Guan H, Xue H, Lu X and Li Y (2019) Experimental study on the progressive
461 collapse behaviour of RC flat plate substructures subjected to corner column removal scenarios.
462 *Engineering Structures* **180**: 728-741.

463 Ma F, Gilbert BP, Guan H, Lu X and Li Y (2020) Experimental study on the progressive collapse
464 behaviour of RC flat plate substructures subjected to edge-column and edge-interior-column
465 removal scenarios. *Engineering Structures* **209**: 110299.

466 Muttoni A (2008) Punching shear strength of reinforced concrete slabs without transverse
467 reinforcement. *ACI Structural Journal* **105(4)**: 440-450.

468 Peng Z, Orton SL, Liu J and Tian Y (2017) Experimental study of dynamic progressive collapse in
469 flat-plate buildings subjected to exterior column removal. *Journal of Structural Engineering*
470 **143(9)**: 04017125.

Peng Z, Orton SL, Liu J and Tian Y (2018) Experimental study of dynamic progressive collapse in flat-plate buildings subjected to an interior column removal. *Journal of Structural Engineering* **144(8)**: 04018094.

Qian K, Liang SL, Fu F and Li Y (2021) Progressive collapse resistance of emulative precast concrete frames with various reinforcing details. *Journal of Structural Engineering* **147(8)**: 04021107.

Qian K and Li B (2013) Experimental study of drop panel effects on response of reinforced concrete flat slabs after loss of corner column. *ACI Structural Journal* **110(2)**: 319–329.

Qian K and Li B (2015b) Dynamic disproportionate collapse in flat-slab structures. *Journal of Performance of Constructed Facilities* **29(5)**: B4014005.

Qian K and Li B (2015a) Load-resisting mechanism to mitigate progressive collapse of flat slab structures. *Magazine of concrete research* **67(7)**: 349-363.

Qian K and Li B (2015c) Strengthening of multibay reinforced concrete flat slabs to mitigate progressive collapse. *Journal of Structural Engineering* **141(6)**: 04014154.

Qian K and Li B (2016) Resilience of flat slab structures in different phases of progressive collapse." (2016). *ACI Structural Journal* **113(3)**: 537-548.

Qian K, Weng YH, and Li B (2018) Impact of two columns missing on dynamic response of RC flat slab structures. *Engineering Structures* **177**: 598-615.

Qian K, Li JS, Huang T, Weng YH and Deng XF (2022a) Punching shear strength of corroded reinforced concrete slab-column connections. J*ournal of Building Engineering* **45**: 103489.

Qian K, Liu JG, Yu XH and Weng YH (2022b) September. Experimental and numerical investigation of punching shear capacity of corroded reinforced concrete slab-column

connections. *Structures* **43**: 1548-1557.

Qian K, Weng YH, Liang SL and Fu F (2024) Punching shear behavior and corrosion resistance of composite slab-column connections reinforced by BFRP and steel rebar. *Engineering Structures* **304**: 117589.

Russell JM, Owen JS and Hajirasouliha I (2015) Experimental investigation on the dynamic response of RC flat slabs after a sudden column loss. *Engineering Structures* **99**: 28-41.

Wang Y, Zhang B, Gu X and Lin F (2022) Experimental and numerical investigation on progressive collapse resistance of rc frame structures considering transverse beam and slab effects. *Journal of Building Engineering* **47**: 103908.

Weng Y, Qian K, Fu F and Fang Q (2020) Numerical investigation on load redistribution capacity of flat slab substructures to resist progressive collapse. *Journal of Building Engineering* **29**: 101109.

Weng YH, Fu F and Qian K (2023) Punching shear resistance of corroded slab–column connections subjected to eccentric load. *Journal of Structural Engineering* **149(1)**: 04022219.

Weng YH, Hu ZJ and Qian K (2025) Punching shear behavior of full-scaled reinforced concrete slab-column connection after cooling from fire-induced elevated temperature. *Engineering Structures* **334**: 120216.

Wu, Y, Crawford, JE and Magallanes, JM (2012) Performance of LS-DYNA Concrete Constitutive Models. *12th Int. LS - DYNA Users Conf* Livermore, CA, 2012.

Xue H, Gilbert BP, Guan H, Lu X, Li Y, Ma F and Tian Y (2018) Load transfer and collapse resistance of RC flat plates under interior column removal scenario. *Journal of Structural Engineering* **144(7)**: 04018087.

Yi WJ, Yi F and Zhou Y (2021) Experimental studies on progressive collapse behavior of rc frame structures: advances and future needs. *International Journal of Concrete Structures and Materials* **15(1)**: 31.

Yi F, Yi WJ, Sun JM, Zhou Y, Zhang WX and He QF (2024) Experimental study on progressive collapse behavior of frame structures triggered by impact column removal. *Engineering Structures* **321**: 119022.

Yi WJ, Zhang FZ and Kunnath SK (2014) Progressive collapse performance of RC flat plate frame structures. Journal of Structural Engineering **140(9)**: 04014048.

Zhang Q and Li YZ (2020) Experimental and modeling study on the progressive collapse resistance of a reinforced concrete frame structure under a middle column removal scenario. *Structural Design of Tall and Special Buildings* **29(2)**: 1693.

527 **Table 1.** Parameters of reinforcement plasticity model.

Parameter type	Value
BETA	1.0
SRC	3.2
SRP	5.0

528 Note: BETA = Hardening parameter; SRC = Strain rate parameter, C, for Cowper Symonds strain

529 rate model; SRP = Strain rate parameter, P, for Cowper Symonds strain rate model.

530

531 **Table 2.** Comparison between Test and FEM values.

Specimen	Date	Inflection point displacement (mm)	Steady displacement (mm)
B1	TEST	29.0	28.0
	FEM	28.6	28.6
	Error	1.4%	2.1%
B2	TEST	156.0	154.4
	FEM	152.5	157.0
	Error	2.2%	1.7%

532

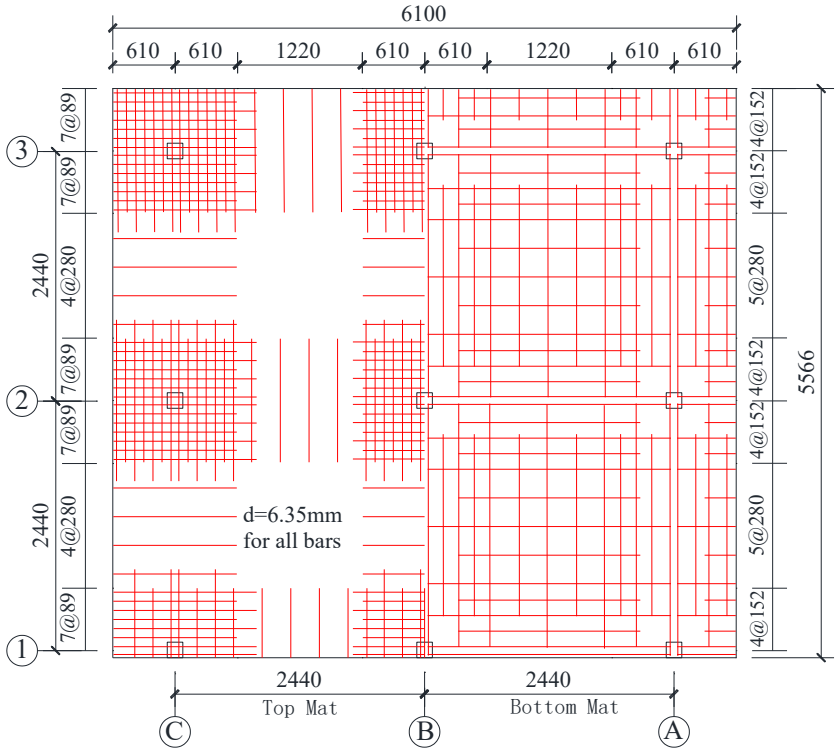

533

534 **Figure 1.** Dimensions and reinforcement of specimen (Unit in mm).

535

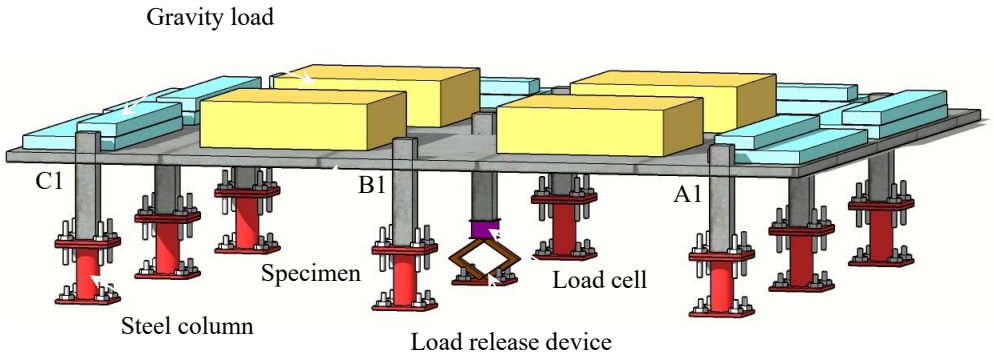

536

537 **Figure 2.** Test setup.

538

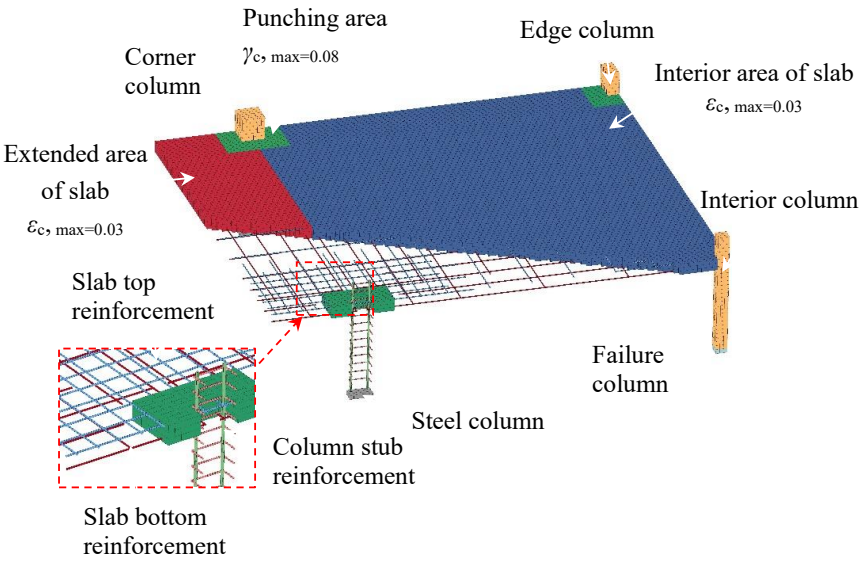

539

540 **Figure 3.** Numerical model (Only a quarter shown due to symmetry).

541

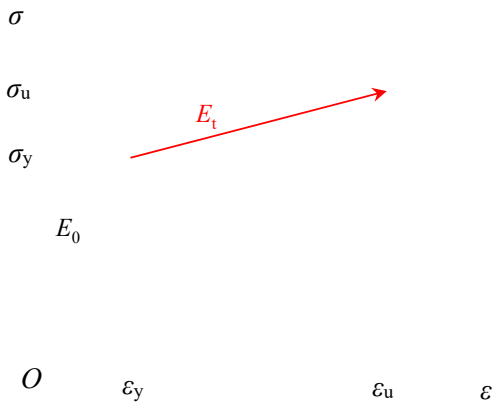

542

543 **Figure 4.** Bilinear elastic-plastic model of reinforcement.

544

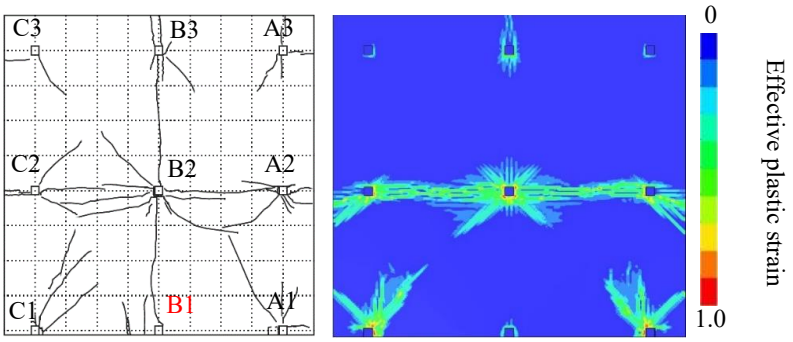

Figure 5. Comparison of numerical and experimental results (Peng *et al*. 2017) for the top surface slab cracks after the removal of Column B1.

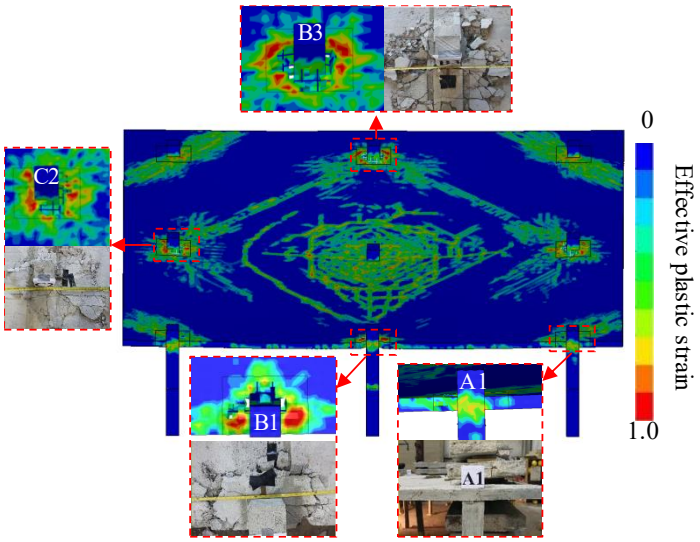

Figure 6. Comparison of numerical and experimental results(Peng *et al*. 2018) for the top surface slab cracks after the removal of Column B2.

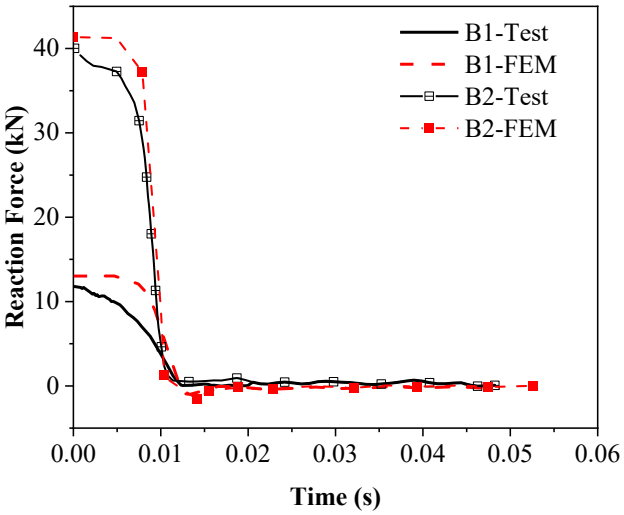

553

554 **Figure 7.** Comparison of numerical and experimental results for the reaction force-

555 time history of the removed column.

556

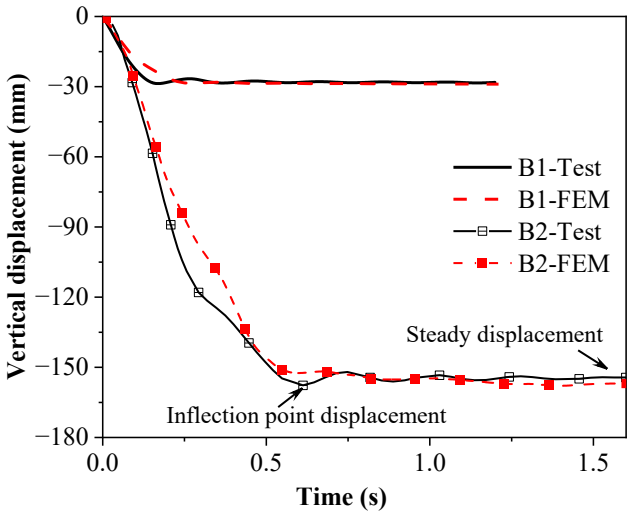

557

558 **Figure 8.** Comparison of numerical and experimental results for the vertical

559 displacement-time history of the removed column.

560

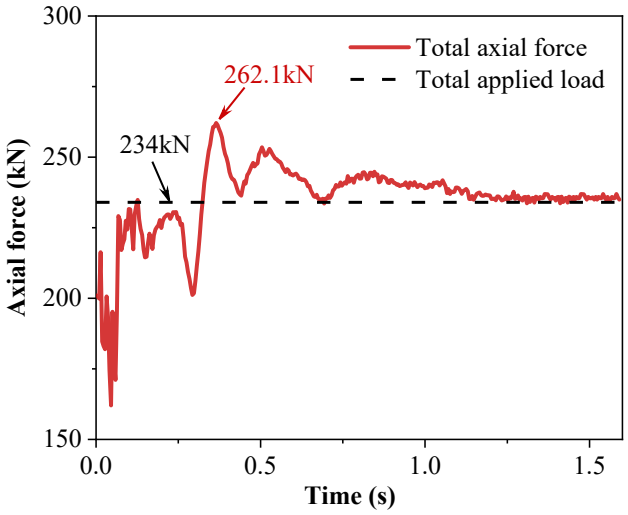

561

562 **Figure 9.** Time history of total axial force in columns

563

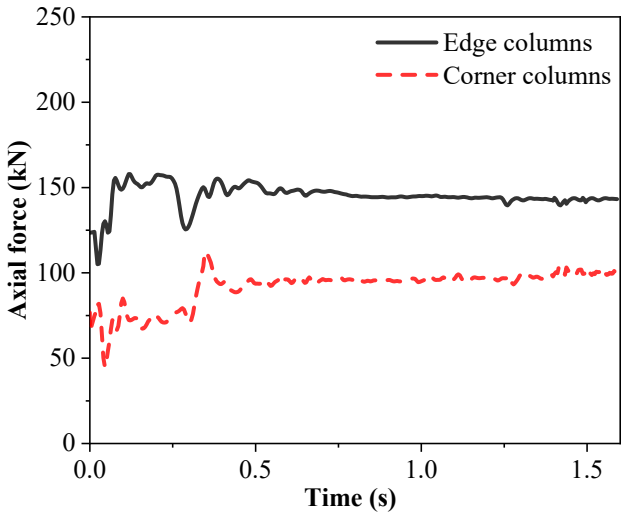

564

565 **Figure 10.** Time-history of the change of axial force in edge and corner columns.

566

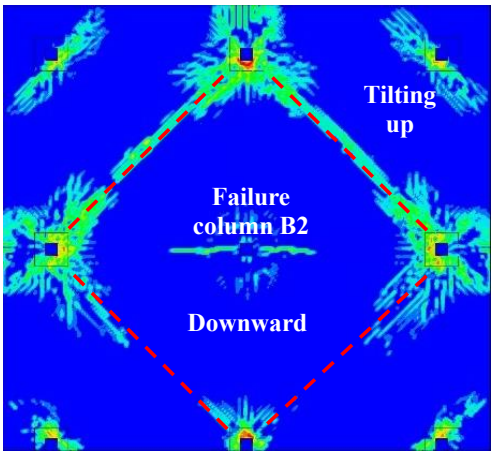

Figure 11. Simulation of structural deformation.

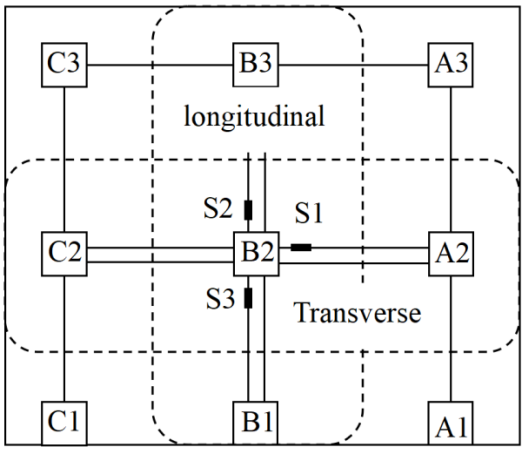

Figure 12. Critical sections within the slab.

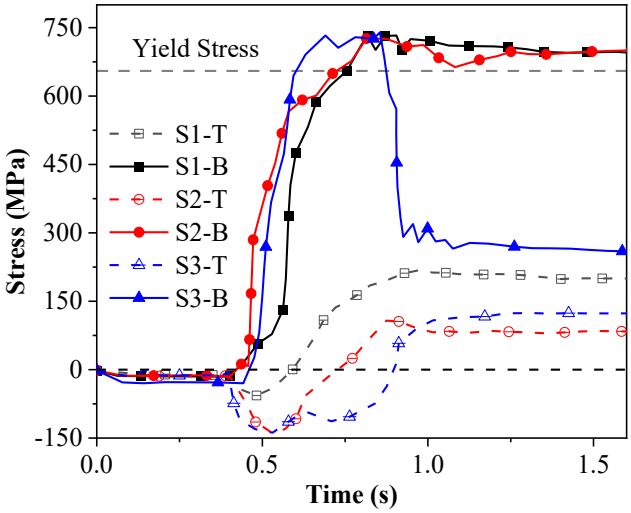

573

574 **Figure 13.** Reinforcement stress at sections.

575

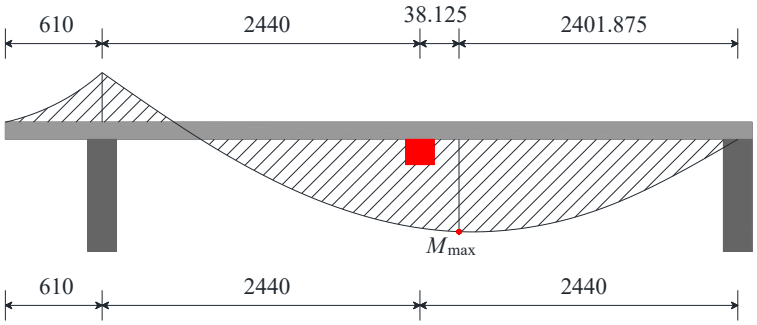

576

577 **Figure 14.** Bending moment distribution of the structural.

578

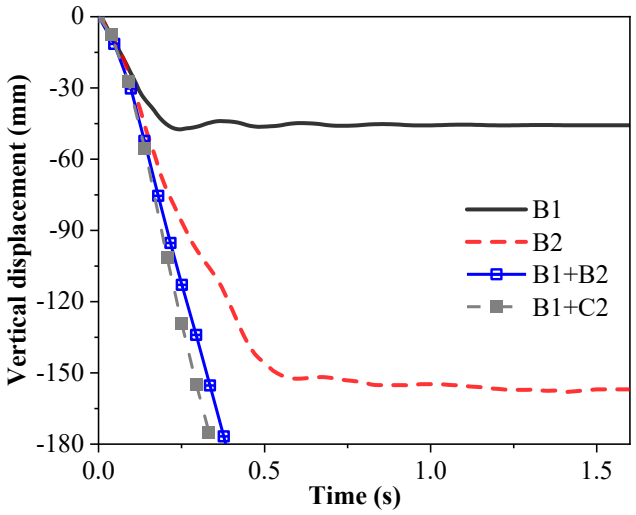

579

580 **Figure 15.** Vertical displacement-time curves under different column removal scenarios.

581

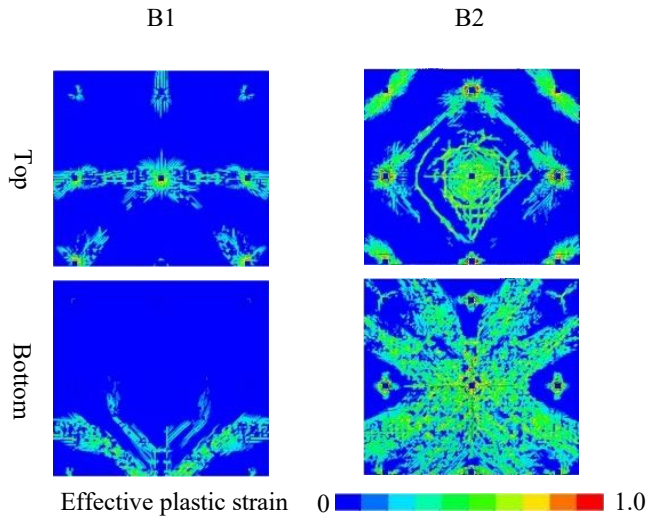

582

583 **Figure 16.** Crack pattern after removal of columns B1 and B2.

584

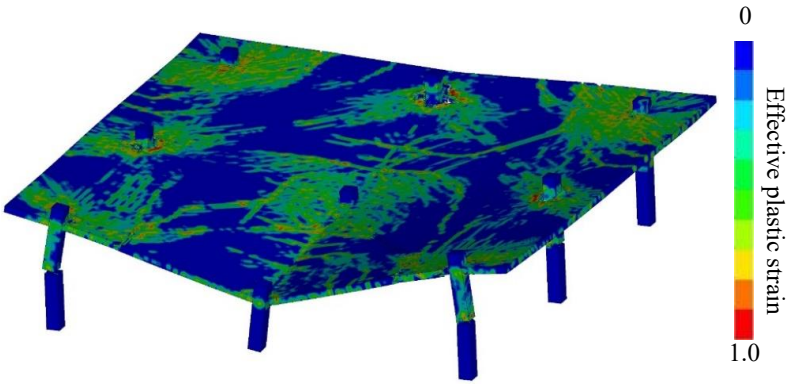

585

586 **Figure 17.** Failure mode after removal of columns B1+B2.

587

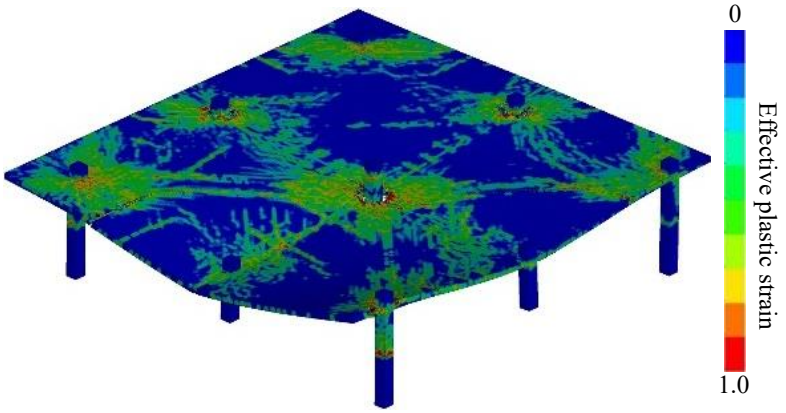

588

589 **Figure 18.** Failure mode after removal of columns B1+C2.

590

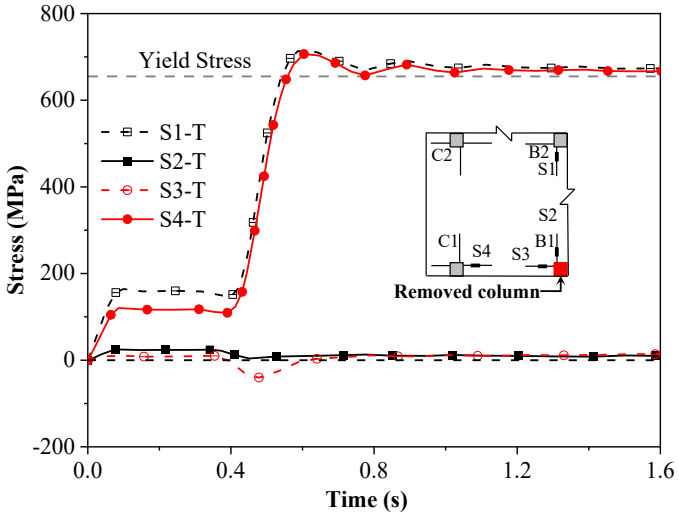

591

592 (a) Top of the slab

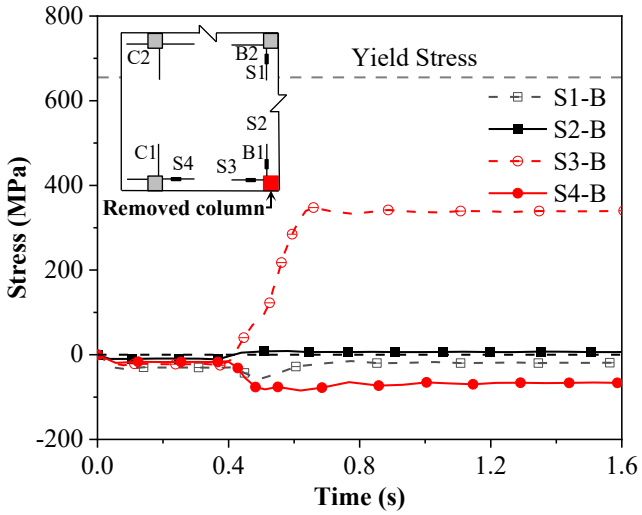

593

594 (b) Bottom of the slab

595 **Figure 19.** Reinforcement stress after removal of column B1.

596

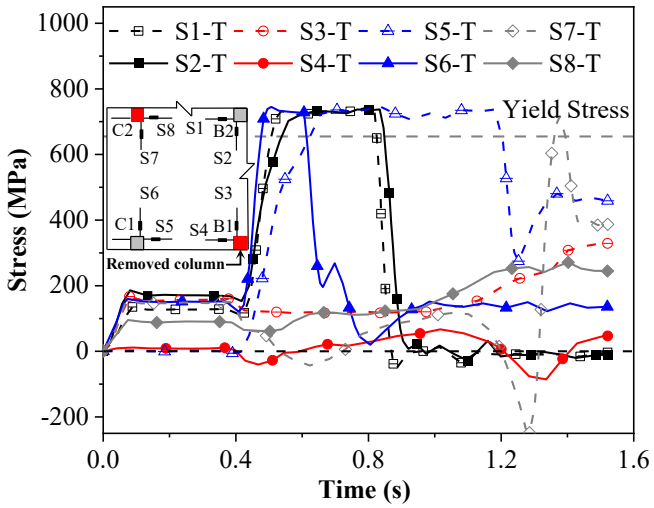

(a) Top of the slab

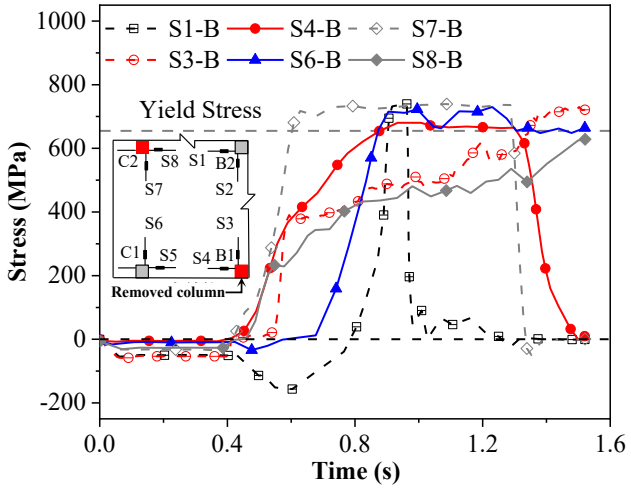

(b) Bottom of the slab

Figure 20. Reinforcement stress after removal of columns B1+C2.

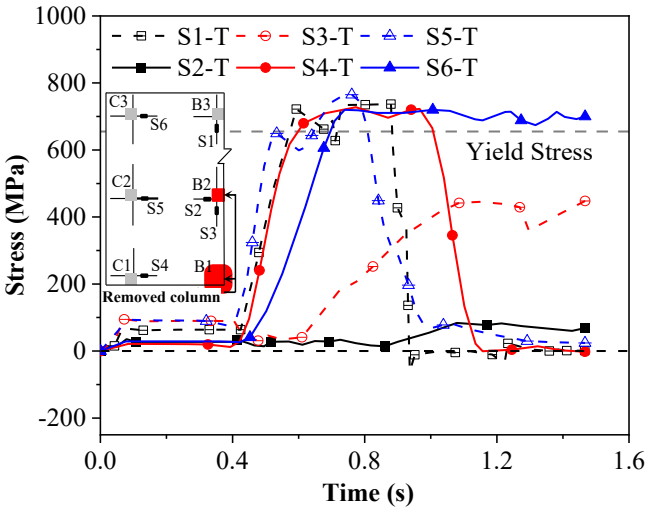

603

604 (a) Top of the slab

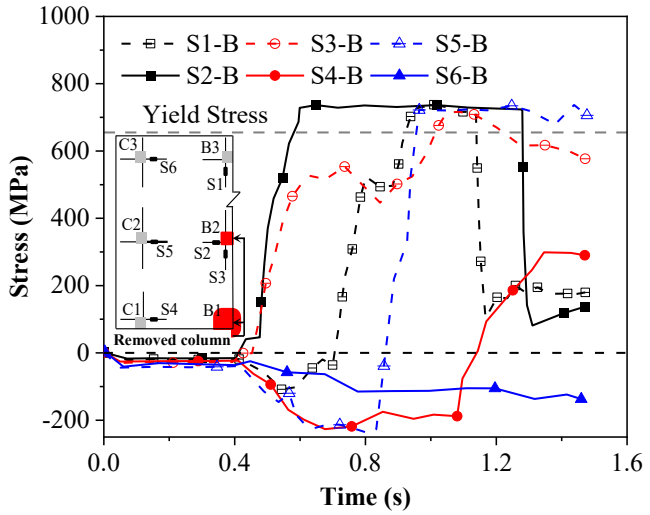

605

606 (b) Bottom of the slab

607 **Figure 21.** Reinforcement stress after removal of columns B1+B2.

608

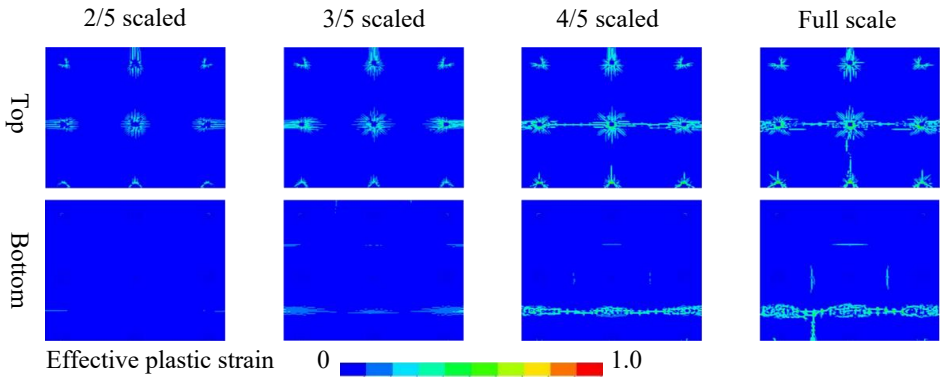

609

610 **Figure 22.** Initial damage before column failure of different structural sizes.

611

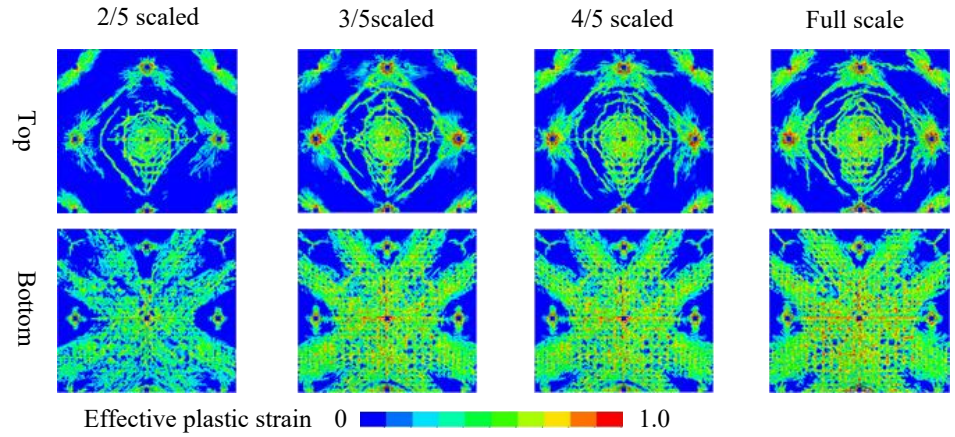

612

613 **Figure 23.** Simulated crack pattern of different structural sizes.

614

615

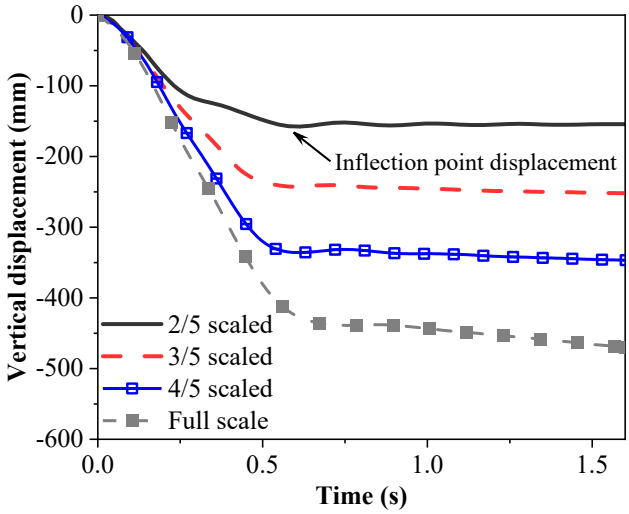

Figure 24. Displacement-history curves.

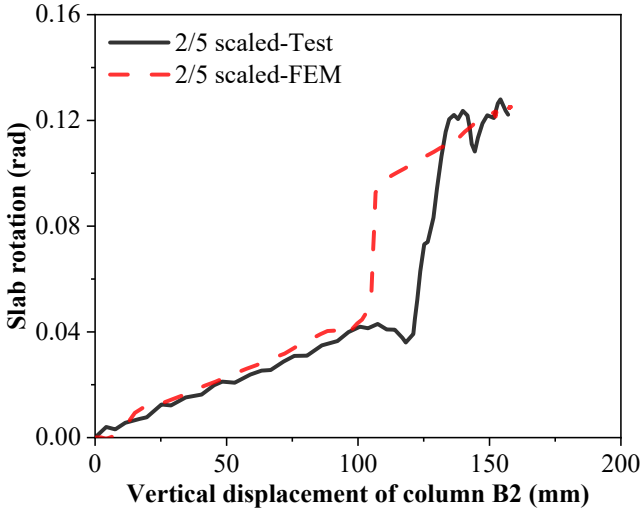

Figure 25. Comparison of numerical and experimental results (Peng *et al*. 2018) for the reaction force-time history of the removed column.

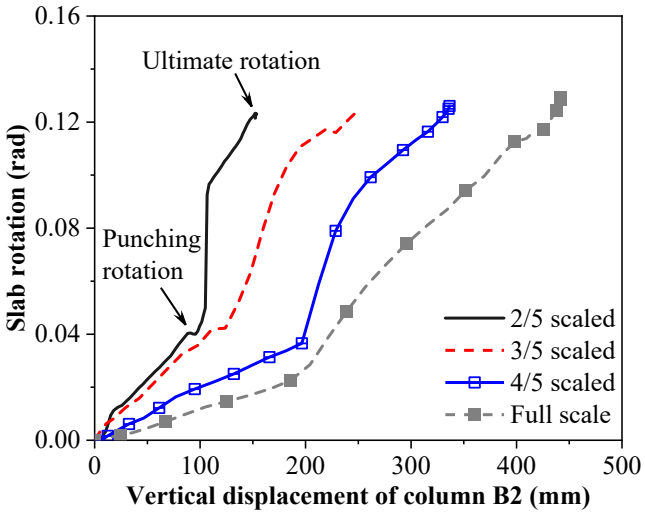

624

625 **Figure 26.** Slab rotation relative to column versus vertical displacement at Column

626 B2 under different scale ratio.

627

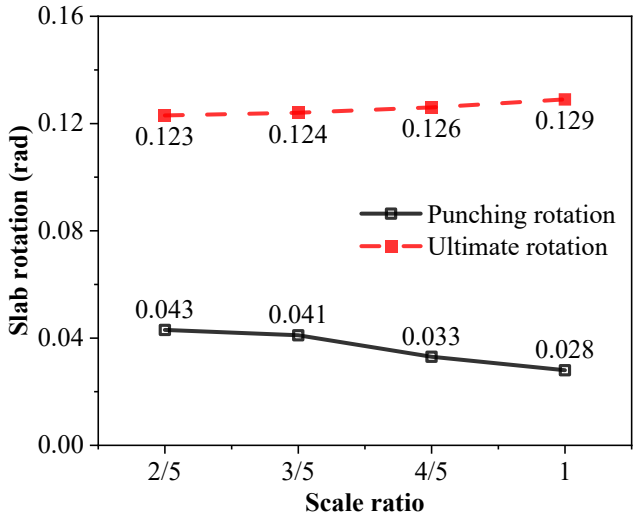

628

629 **Figure 27.** Slab rotation relative under different scale ratio.

630

631

632

633